

Osteoarthritis and Cartilage



Development of a cyclic-inverso AHSG/Fetuin A-based peptide for inhibition of calcification in osteoarthritis



G.G.H. van den Akker †, J.S.J.J. Steijns †^a, R.H.M.J. Stassen †^a, G.B. Wasilewski ‡, L.C.W. Peeters †, K.A.P. Wijnands †, L.J. Schurgers ‡, M.M.J. Caron †, L.W. van Rhijn †, T.J.M. Welting †^{*}

† Laboratory for Experimental Orthopedics, Department of Orthopedic Surgery, Maastricht University Medical Centre+, 6229 HX Maastricht, the Netherlands

‡ Department of Biochemistry, Cardiovascular Research Institute Maastricht, Maastricht University, Maastricht, the Netherlands

ARTICLE INFO

Article history:

Received 28 March 2022

Accepted 14 November 2022

Keywords:

Calcification
Osteoarthritis
Peptide
Fetuin A

SUMMARY

Objective: Ectopic calcification is an important contributor to chronic diseases, such as osteoarthritis. Currently, no effective therapies exist to counteract calcification. We developed peptides derived from the calcium binding domain of human Alpha-2-HS-Glycoprotein (AHSG/Fetuin A) to counteract calcification.

Methods: A library of seven 30 amino acid (AA) long peptides, spanning the 118 AA Cystatin 1 domain of AHSG, were synthesized and evaluated in an *in vitro* calcium phosphate precipitation assay. The best performing peptide was modified (cyclic, retro-inverso and combinations thereof) and evaluated in cellular calcification models and the rat Medial Collateral Ligament Transection + Medial Meniscal Tear (MCLT + MMT) osteoarthritis model.

Results: A cyclic peptide spanning AA 1–30 of mature AHSG showed clear inhibition of calcium phosphate precipitation in the nM–pM range that far exceeded the biological activity of the linear peptide variant or bovine Fetuin. Biochemical and electron microscopy analyses of calcium phosphate particles revealed a similar, but distinct, mode of action in comparison with bFetuin. A cyclic-inverso variant of the AHSG 1–30 peptide inhibited calcification of human articular chondrocytes, vascular smooth muscle cells and during osteogenic differentiation of bone marrow derived stromal cells. Lastly, we evaluated the effect of intra-articular injection of the cyclic-inverso AHSG 1–30 peptide in a rat osteoarthritis model. A significant improvement was found in histopathological osteoarthritis score and animal mobility. Serum levels of IFN γ were found to be lower in AHSG 1–30 peptide treated animals.

Conclusions: The cyclic-inverso AHSG 1–30 peptide directly inhibits the calcification process and holds the potential for future application in osteoarthritis.

© 2022 The Author(s). Published by Elsevier Ltd on behalf of Osteoarthritis Research Society International. This is an open access article under the CC BY license (<http://creativecommons.org/licenses/by/4.0/>).

Introduction

Pathological calcification of soft tissues is a key factor in a multitude of chronic diseases, such as atherosclerosis¹, kidney failure² and osteoarthritis³. While the importance of calcium depositions has been well recognized in kidney disorders⁴, this was initially not recognized for atherosclerosis and osteoarthritis (OA)⁵. It has now become clear that calcium-containing crystals, often

difficult to detect in the form of microparticles, can indeed initiate as well as exacerbate disease^{6,7}. Pathological calcifications mostly consist of Basic Calcium Phosphate (BCP) and Calcium Pyrophosphate Dihydrate (CPPD). In OA, both BCP and CPPD are often found in synovium and synovial fluid. Injection of BCP crystals in murine knee joints led to rapid proteoglycan (PG) loss, VDIPEN neopeptide formation and chondrocyte apoptosis⁸. Human articular chondrocytes (HACs) stimulated with BCP or CPPD crystals induced senescence and chondrocyte hypertrophy⁹. Control over calcification is of vital importance in vertebrates, where high concentrations of metal ions and anions, such as inorganic phosphate (Pi), can be found in the intra- and extracellular environment. Calcium ion levels are maintained within stringent boundaries

* Address correspondence and reprint requests to: T.J.M. Welting, Universiteitssingel 50, 6229 ER Maastricht, the Netherlands.

E-mail address: t.welting@maastrichtuniversity.nl (T.J.M. Welting).

^a Contributed equally.

(1.15–1.33 mmol/L) in the blood stream by the parathyroid hormone and calcitonin¹⁰. A wide variety of endogenous inhibitors of calcification are present to avoid pathological calcification. For example, Vitamin K dependent proteins (Upper zone of cartilage and matrix associated protein UCMA, Osteocalcin, Matrix Gla protein (MGP)) are crucially involved in calcification, bone and cartilage homeostasis and associated with osteoarthritis¹¹.

Alpha2-Heremans-Schmid-Glycoprotein (AHSG) is an abundant protein in the circulation (0.4–0.8 mg/ml in human serum¹²) and bone. It has a high calcium ion binding capacity and is noticeably absent in avascular tissue's, such as cartilage¹³. Although discovered in 1944, its crucial function in the inhibition of ectopic calcification was only established with the first knock-out mice that present with excessive calcifications in all soft tissues^{14,15}. AHSG engages calcium-containing particles with its N-terminal Cystatin 1 domain and is estimated to bind calcium ions directly^{16,17}. It can sequester larger amounts of calcium due to the formation of calci-protein particles (CPP), which contain up to 25% AHSG and 75% minerals (v/v)¹³. Primary CPPs (50–100 nm) have a core of amorphous calcium phosphate, while the larger secondary CPPs (>100 nm) contain hydroxyapatite crystals¹⁸. Primary CPPs protect against undesirable calcification and can be absorbed by endothelial cells in the liver and the spleen. Secondary CPPs contribute to pathological calcifications and can be scavenged by macrophages¹⁹. Serum AHSG levels are decreased by inflammation in chronic kidney disorders (CKD)^{20,21}. As such AHSG is thought to play an important role in pathological calcification resulting from the metabolic syndrome and CKD. In vascular calcification it is not clear whether or not circulating AHSG levels are involved^{22,23}. On the other hand, we found increased AHSG levels in synovial fluid derived from end-stage OA patients compared to healthy controls²⁴. The presence of BCP or CPPD crystals in synovial fluid was associated with higher AHSG expression in OA patients²⁵. Previously, short calcium binding peptides of 2–14 amino acids (AA) have been identified using enzymatic digestions or

hydrolysis of proteins for, amongst others, dietary supplementation purposes^{26–30}. It is not known whether calcium binding peptides can be harnessed to prevent calcification. In this study, we aimed to develop peptides derived from the Cystatin 1 domain of the most potent calcium ion and CPP binding protein AHSG, as a strategy to reduce pathologic calcification in OA.

Methods

Peptide synthesis

Lyophilized peptides were synthesized by PepScan (Lelystad, the Netherlands) and dissolved based on amino acid content. AA sequences are presented in Table I.

In vitro calcium phosphate precipitation assay

Calcium precipitation assays were performed essentially as described before with minor adaptations³¹. 2.4 mM calcium chloride (0.1 M stock) was added to a 50 mM Tris/HCl buffer (pH 7.4) in 1.5 ml Eppendorf tubes. Peptides were added at indicated concentrations and incubated for 15 min. Subsequently, 1.6 mM phosphate buffer (0.1 M stock) was added and the mixture was incubated for 120 min at 37°C. Samples were transferred to cuvettes and A620 was measured (Novaspec Plus, Amersham Biosciences, Roosendaal, the Netherlands). Modifications to this protocol are indicated in the figure legend.

Scanning Electron Microscopy

In vitro calcium precipitation reactions were stopped by transferring samples to dialysis membranes (Sigma D9777, Zwijndrecht, the Netherlands). Precipitates were freeze-dried, mounted on aluminum stubs and gold-coated prior to Scanning Electron

Fig. 1 (crude synthesis)

Amino acid sequence (N to C terminus)
AHSG 1–30
AHSG 16–45
AHSG 31–60
AHSG 46–75
AHSG 61–90
AHSG 76–105
AHSG 91–120

Figs. 2–6 & supplement (purified)

Amino acid sequence (N to C terminus)
AHSG 1–30
AHSG 1–30 cyclic (Cyc.)
AHSG 1–30 Cyc. inverse (C.I.)
AHSG 1–30 – D–N/E–Q
AHSG 1–30 – alphabetical order
AHSG_3–32
AHSG_5–34
AHSG_7–36
AHSG_9–38
AHSG_11–40
AHSG_13–42
AHSG_15–44
AHSG_17–46
AHSG 46–75

Table I

Peptide nomenclature and amino acid sequences

Osteoarthritis and Cartilage

Microscopy (SEM) investigation (Scios, Thermo-Fisher, Bleiswijk, the Netherlands). Images were obtained at 10.0 kV and 0.40 nA.

Calcium and phosphate assays

Samples were hydrolyzed in 0.1 M HCl and total calcium content was quantified with the Radox assay (London, United Kingdom) or used to quantify total phosphate with a phosphate colorimetric assay (Sigma, MAK-030, Zwijndrecht, the Netherlands). Next, cell samples were neutralized with 0.1 M NaOH and 0.1% SDS was added to determine total protein content (micro DC Protein Assay, Thermo Scientific, Bleiswijk, the Netherlands) for normalization.

Cellular calcification models

Human vascular smooth muscle cells (VSMCs) were isolated from human aortic samples. Ten-thousand cells per cm^2 were seeded for experiments. After 24 h medium was changed to calcification medium (growth medium with 4.5 mM calcium or 4.5 mM calcium with peptides at indicated concentrations). Media were refreshed every second or third day until visual confirmation of calcification at day 7. HACs were isolated from surgical

waste material of total knee replacement surgery of end-stage osteoarthritis patients after informed consent (METC (Medical Ethical Committee) 2017-0183). Thirty-thousand cells per cm^2 were seeded for experiments and after 24 h medium was changed to calcification medium (growth medium with 1 mM Adenosine TriPhosphate (ATP) or 1 mM ATP with peptides at indicated concentrations). Media were refreshed every second or third day until visual confirmation of calcification at day 7.

Bone Marrow derived Stromal Cells (BMSCs) were isolated from bone marrow aspirates from the iliac crest of young individuals (METC 08-4-056). Osteogenic differentiation was achieved with growth medium, supplemented with ascorbic acid 50 $\mu\text{g}/\text{ml}$, 100 nM dexamethasone and 10 mM beta-glycerolphosphate. Media were refreshed every second or third day until visual confirmation of calcification at day 21. Differentiation was verified by Alizarin red staining³² and gene expression analysis (Supplementary Fig. 2)³³.

Rat osteoarthritis model

The study was conducted via a contract research project at Bolder BioPATH (BBP, Boulder, USA). Lewis rats ($n = 40$) underwent surgery where the medial collateral ligament was transected and a

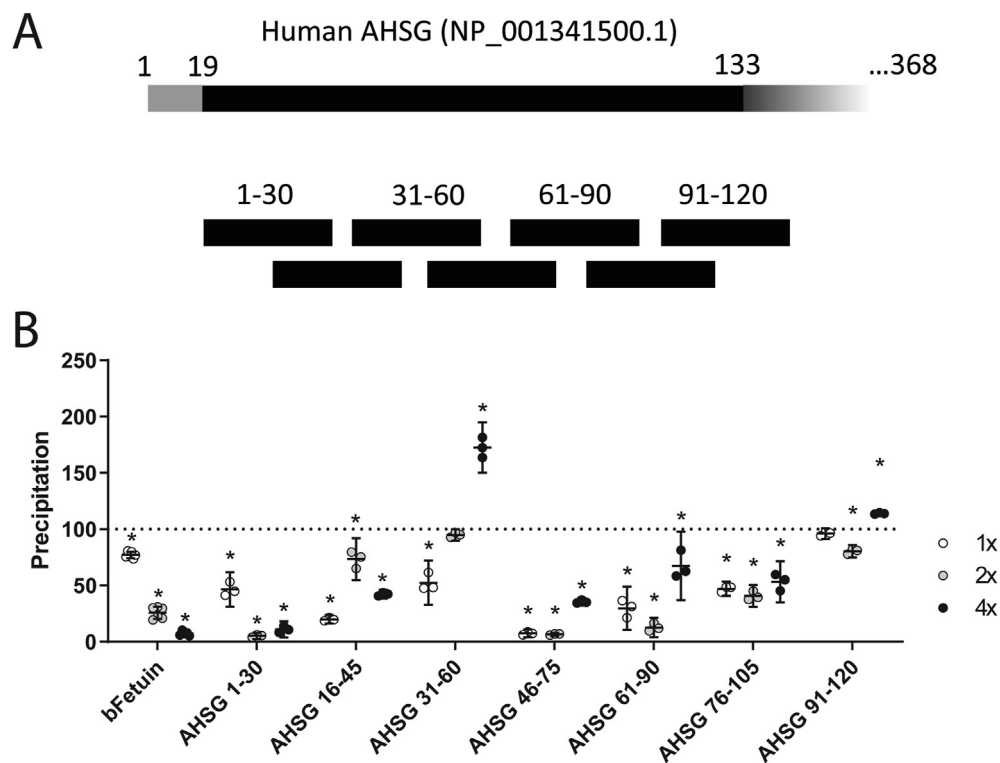


Fig. 1

Osteoarthritis and Cartilage

AHSG Cystatin 1 domain peptide library and screening. A) Design of 30 AA overlapping peptides of the human AHSG Cystatin 1 protein domain. Gray = pre-pro domain, black = Cystatin 1 domain, fading gray = remainder of the 368 AA AHSG protein. Note that the most C-terminal peptide in the library contains 5 AA that lie outside the Cystatin 1 domain. B) Calcium precipitation assay with three increasing concentrations of crude peptide. Bovine Fetuin (bFetuin): 0.25–0.5–1.0 mg/ml = 1×–2×–4× and a 10 fold molar excess of peptide compared to bFetuin (206.7–413.2–826.6 μM = 1×–2×–4×). bFetuin was used as an internal control for the inhibition of calcium precipitation. The positive control was normalized to 100%. * = P value < 0.05 in a one-way ANOVA with Dunnett's post-test when compared to control (dashed line). Mean \pm 95% confidence interval ($n = 3$).

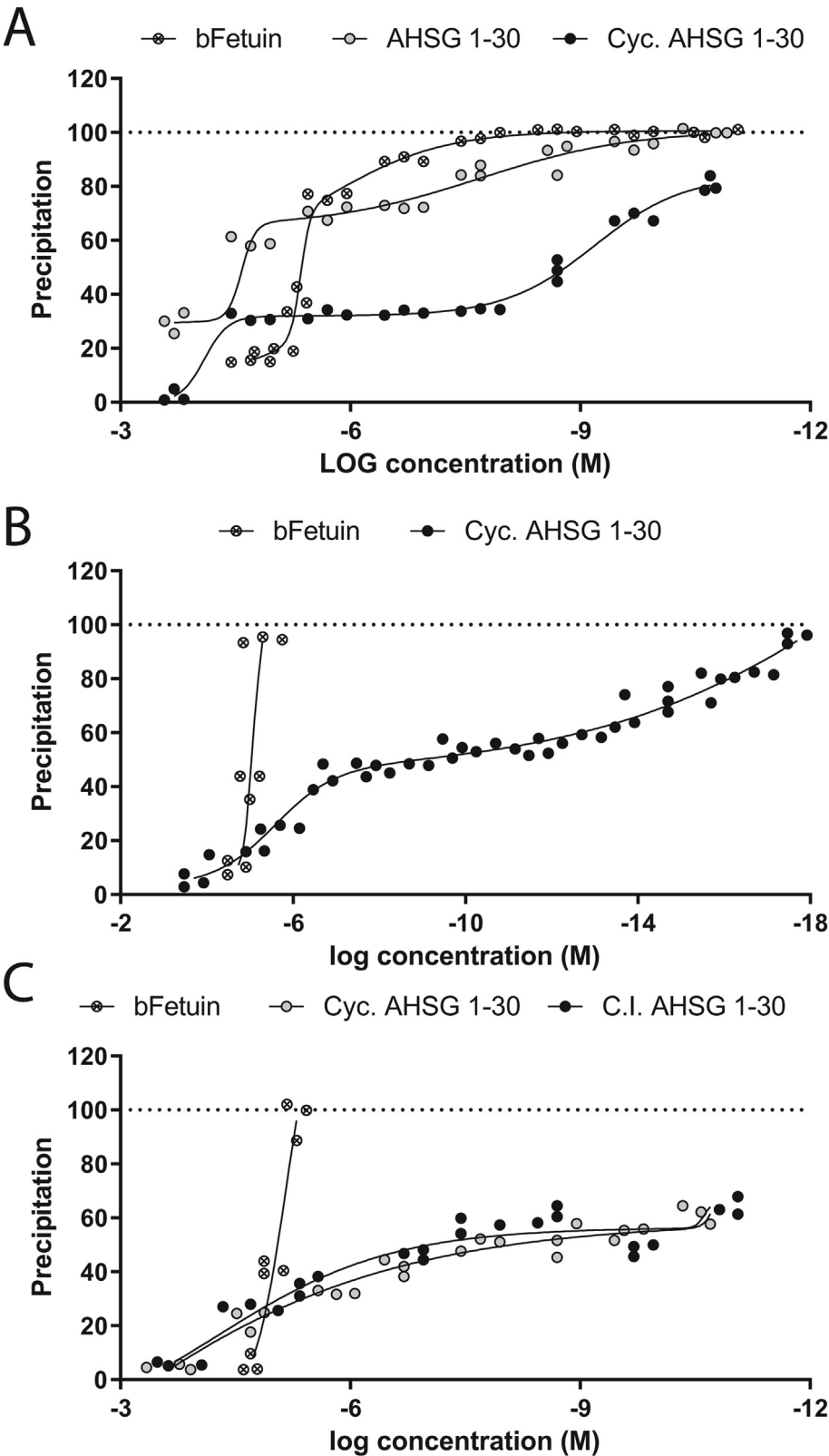
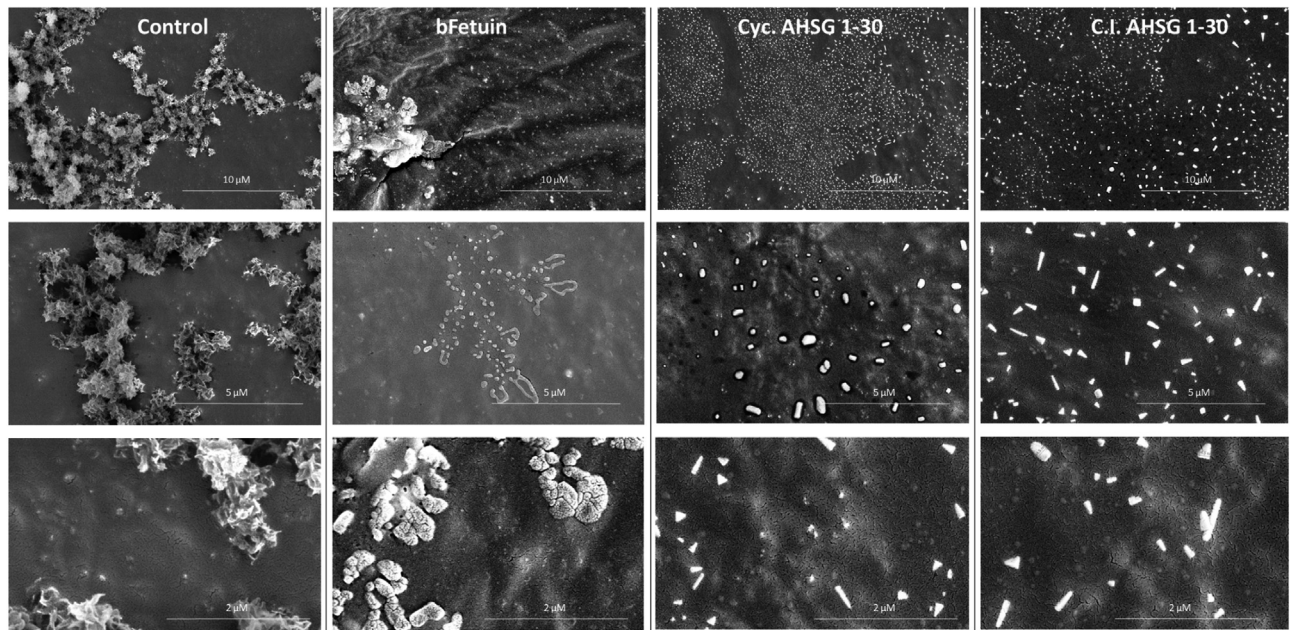


Fig. 2

A



B

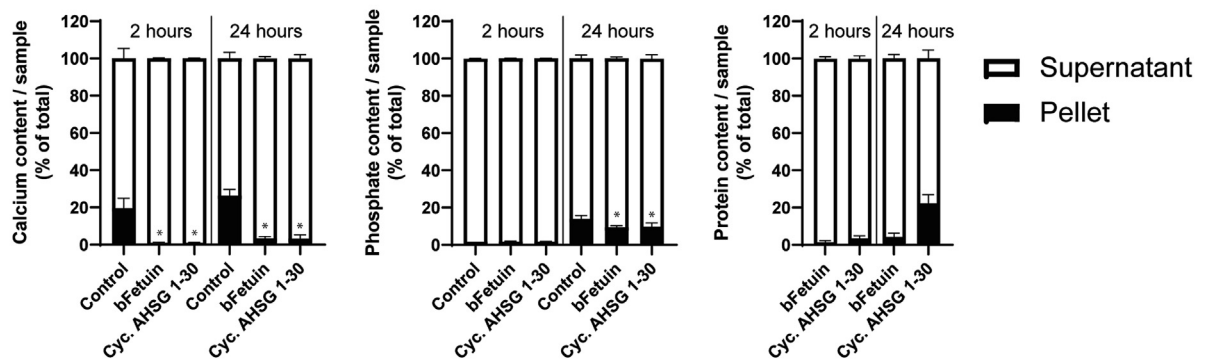


Fig. 3

Osteoarthritis and Cartilage

Cyclic AHSG 1–30 inhibits calcium precipitation through direct interaction with the precipitate. A) Electron microscopy images were obtained from precipitates formed after two hours in the presence or absence of bFetuin (0.5 mg/ml), Cyc. AHSG 1–30 (20.67 nM) or C.I. AHSG 1–30 (20.67 nM). Precipitation inhibition of ~50% was confirmed by absorption measurements prior to sample processing (dialysis). Upper row magnifications: 15.000 \times , middle row: 35.000 \times , bottom row: 100.000 \times , 20.000 \times and 50.000 \times (Control, bFetuin, Cyc. AHSG 1–30 and C.I. AHSG 1–30). Bottom row images were enlarged and cropped to the same size. The Cyc. and C.I. AHSG 1–30 derived particles were susceptible to dissolution by the electron beam at high magnification (>35.000 \times). B) Calcium precipitates were allowed to form for 2 or 24 h in the presence or absence of bFetuin (0.5 mg/ml) or Cyc. AHSG 1–30 (20.67 nM). Precipitation inhibition of ~50% was confirmed by absorption measurements prior to sample processing. Total calcium, phosphate and protein levels were determined in the supernatant and pellet of each sample and normalized to 100%. Statistical comparisons were done using a Student *t*-test between Control and bFetuin or Control and Cyc. AHSG 1–30. * = *P* value < 0.05. Mean \pm 95% confidence interval (*n* = 4).

Cyclization of AHSG 1–30 enhances precipitation inhibitory capacity. A) Precipitation inhibition capacity of a dilution series of linear AHSG 1–30 and a cyclic variant (Cyc.) of the peptide (206.7 μ M–20.67 μ M). B) Precipitation inhibition capacity of a dilution series in steps of 10 of the Cyc. AHSG 1–30 peptide. C) Precipitation inhibition capacity of a dilution series in steps of 10 (total 108) of Cyc. AHSG 1–30 and its inverso (D-amino acids) variant (C.I.). bFetuin (0.25–0.5–1.0 mg/ml) was used as an internal control for the inhibition of calcium precipitation. The positive control was normalized to 100% (dashed line). Individual data points are shown in a staggered manner to avoid overlapping data points (*n* = 3 per bFetuin or peptide concentration).

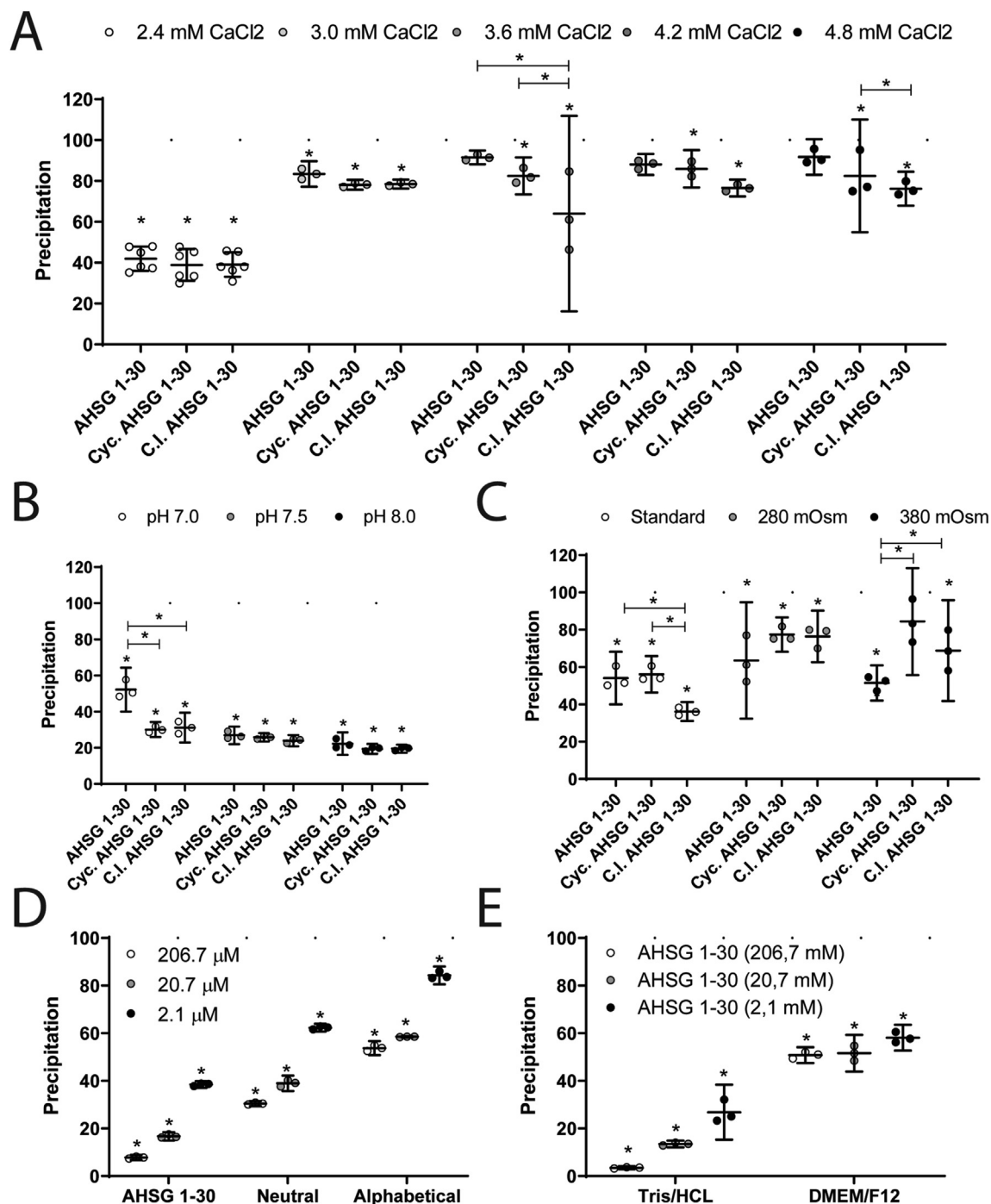


Fig. 4

The sequence of the AHSG 1–30 peptide is more important than its negatively charged amino acids and it is less effective in solutions with higher calcium ion concentrations, lower pH or increased osmolarity. A) The effect of supra-physiological concentrations of calcium ions on the precipitation inhibition of the linear, Cyclic and C.I. AHSG 1–30 peptide [20.67 μ M] were evaluated. B) The effect of upper and lower limits of physiological pH on precipitation inhibition were evaluated for the indicated peptide variants at 20.67 μ M. C) The effect of different osmolarity was evaluated for the three indicated peptide variants at 20.67 μ M. Osmolarity was calculated to be 62 mOsm based on the known composition of the solution. To increase osmolarity, we utilized a 5 M sodium chloride stock solution as described earlier. D) The linear AHSG 1–30 peptide was compared with a D to N and E to Q substituted variant (labeled D–N/E–Q) and a peptide with alphabetically ordered amino acids (labeled “alphabetical”) at indicated concentrations. E) The calcium phosphate precipitation assay in Tris/HCL buffer was repeated in DMEM/F12 at indicated peptide concentrations. The same amount of calcium and phosphate was added to these solutions. A precipitation inhibition test of a two amino acid library of AA 1–46 can be found in [Supplemental Fig. 1](#). Statistical comparisons were made using two-way ANOVA with Bonferroni post-tests. * = P value < 0.05. The asterisk denotes a comparison with the positive control in the same condition unless indicated otherwise. Mean \pm 95% confidence interval (n = 3).

single full thickness cut was made through the meniscus in the right knee joint³⁴. Sample size of 18 per group was calculated according to the formula $n_i(\text{sample size}) = 2 * (((Z1 - \alpha/2) + (Z1 - \beta)) / ES)^2$ with alpha 0.05 and power of 0.80, which was based on earlier experience with this model³⁵ and data obtained for *in vitro* HAC calcification and corrected for a potential drop-out of 10% (2 animals). Intra-articular injection of 50 μ l saline ($n = 20$) or C.I. AHSG 1–30 (20 μ M; $n = 20$) was performed on days 7, 10, 14, 17, 21 and 24 post-surgery. Gait analysis was performed at day 20 by applying ink to the ventral surface of the foot and documenting weight bearing during movement (footprints) across paper. Rear feet of rats were placed in ink, then rats were placed on paper and allowed to walk the full length. Gait was scored visually as described earlier³⁶. At day 28 post-surgery, animals were bled to exsanguination by descending aorta blood draw followed by bilateral thoracotomy. Whole blood was processed to serum, which was stored frozen at -80°C . Knee joints were embedded in paraffin and stained histological sections with toluidine blue and scanned images were used to perform OA scoring³⁷ and rat specific OA scoring³⁸ by two blinded observers that were allowed to confer. Immunohistochemical analyses was essentially performed as described earlier³⁹. Controls and additional details can be found in [Supplementary Fig. 3](#). Stained slides were mounted and scanned with an M8 Pre-Cipoint microscope. A rat cytokine 23-plex assay (Bio-Rad #12005641) was used on a Bio-Plex 200 system (Bio-Rad). Rat CRP was determined by ELISA (Invitrogen, Cat. No. 88-7501-28). ALP activity was determined as described earlier³⁵ and normalized to protein concentration (BCA (Bicinchoninic acid assay) assay).

Statistical analyses

The D'Agostino & Pearson test was used to assess normal distribution of the data and groups were compared using either a two-tailed Student *t* test or a Mann–Whitney *U* test. For multiple group comparisons a one way ANOVA with Dunnett's or Bonferroni post-test was used as indicated in the figure legends. Statistical analysis was performed in Graphpad Prism 8.

Results

Cyclic AHSG 1–30 peptide as potent inhibitor of calcification *in vitro*

We designed seven peptides of thirty AA length with fifteen AA overlap covering the entire human Cystatin 1 domain [Fig. 1(A)]. To evaluate the inhibitory capacity of these peptides we utilized an *in vitro* calcium phosphate precipitation assay^{16,17,31}. Six out of seven peptides altered precipitation with the exception of the last AHSG 90–120 peptide. Five peptides consistently inhibited precipitation by 46–62%, while AHSG 31–60 unexpectedly stimulated precipitation. AHSG 1–30 showed the most consistent inhibition upon increasing its concentration [up to 89% inhibition at 0.83 mM; Fig. 1(B)]. Some peptides, most notably AHSG 46–75, showed a better initial inhibition, which turned into less inhibition at higher concentrations. Other peptides showed highly variable results.

To test whether we could improve the potency of the AHSG 1–30 peptide, we designed a cyclic (Cyc.) variant of the linear AHSG 1–30 peptide. A constrained cyclic motif can help reducing unfavorable thermodynamic profiles⁴⁰. bFetuin lost its inhibitory effect at 0.65–2.6 μ M (31.3–125 μ g/ml), while the linear peptide maintained 20% inhibition until ~162.5 nM [Fig. 2(A)]. The Cyc. peptide variant out-performed the linear peptide substantially and maintained 20–50% precipitation inhibition in the pico and nanomolar range. Next, we set out to dilute the Cyc. peptide until it was no longer effective [Fig. 2(B)]. We found that even 20.6 aM, but not 2.6 aM was able to inhibit calcium phosphate precipitation compared

to control [Fig. 2(B)]. Finally, we combined the effective cyclic design with more stable D-amino acids leading to a cyclic inverso (C.I.) peptide variant. Changing AA chirality did not affect the efficient inhibition of precipitation [Fig. 2(C)].

Cyclic AHSG 1–30 peptide incorporated in precipitates and inhibits growth

To obtain insight into the mode of action of the peptide, we analyzed precipitates from the *in vitro* assay using SEM. In the control condition, we found relatively large (~1 μ m) and small (50–200 nm) particles [Fig. 3(A); Control panels]. The larger particles had a distinct morphology that is typical for BCP crystals⁴¹. The bFetuin derived particles had an entirely different morphology that lacked sharp edges [Fig. 3(A)]. These particles also appeared to be somewhat smaller (~0.5 μ m). The Cyc. AHSG 1–30 and C.I. AHSG 1–30 derived particles appeared even smaller and more compact. They had triangular, squared or in rare cases penta- or hexagonal morphologies [Fig. 3(A)]. No difference was found in shape and morphology between Cyc. AHSG 1–30 or C.I. AHSG 1–30 particles. The smallest discernable particles from the peptide treated sample had a size of 67 nm \pm 7 (Mean \pm SD, $n = 4$), which could resemble primary CPP (<100 nm). This was not the case for particles in the control sample. Since it is known that AHSG prevents CPP growth by covering its outer surface, we hypothesized that our peptide also interacts with the calcium phosphate particles. The amount of calcium in control pellets remained similar over time [Fig. 3(B); left panel]. The amount of precipitated calcium did increase as a function of time in bFetuin derived pellets from <1% to >2%. This was still significantly lower than in the positive control. Phosphate content in the pellets increased from 2% to 14% in control pellets. Addition of bFetuin or Cyc. AHSG 1–30 significantly reduced phosphate content to 9% at 24 h [Fig. 3(B); middle panel]. Finally, total protein content measurements established that both bFetuin and Cyc. AHSG 1–30 were incorporated in the pellets [Fig. 3(B); right panel].

Critical determinants of precipitation inhibition by the Cyc. AHSG 1–30 peptide

In a series of direct comparisons between linear, Cyc. and C.I. AHSG 1–30, we varied calcium ion concentration (2.4–4.8 mM), pH (7.0–8.0) or osmolarity (assay osmolarity (62 mOsm), 280 mOsm and 380 mOsm). Higher calcium ion concentrations reduced the effectiveness of bFetuin and the AHSG 1–30 peptide variants [Fig. 4(A)]. The C.I. AHSG 1–30 peptide outperformed the other variants at supra-physiological calcium ion concentrations (3.6–4.8 mM). A pH of 7.0 had a negative effect on the efficacy of the linear peptide in particular [Fig. 4(B)]. Increasing osmolarity decreased the inhibitory effect of the peptides, although this coincided with a lower signal in the positive controls [Fig. 4(C)]. Subsequently, we tested whether the inhibition of calcium phosphate precipitation was dependent on AA charge or sequence (Table I). The peptide without negatively charged amino acids (D–N/E–Q) only worked 23% less efficient and still significantly inhibited precipitation [Fig. 4(D)]. Alphabetical ordering of the AA had a more profound effect and reduced inhibition by 44%. To corroborate the unique properties of the AHSG 1–30 sequence, we generated eight new overlapping peptides with two AA shifts covering the region 1–46 (Supplementary Fig. 1, Table I). A two AA shift to 3–32 already decreased effectiveness of the peptide by 1.3–2.0 fold in the calcium phosphate precipitation assay, while the AHSG 7–36 peptide had the lowest inhibitory effect. In cell culture medium (DMEM/F12) the maximum inhibition of precipitation induced by 2.4 mM calcium and 1.6 mM phosphate remained 50% [Fig. 4(E)]. The

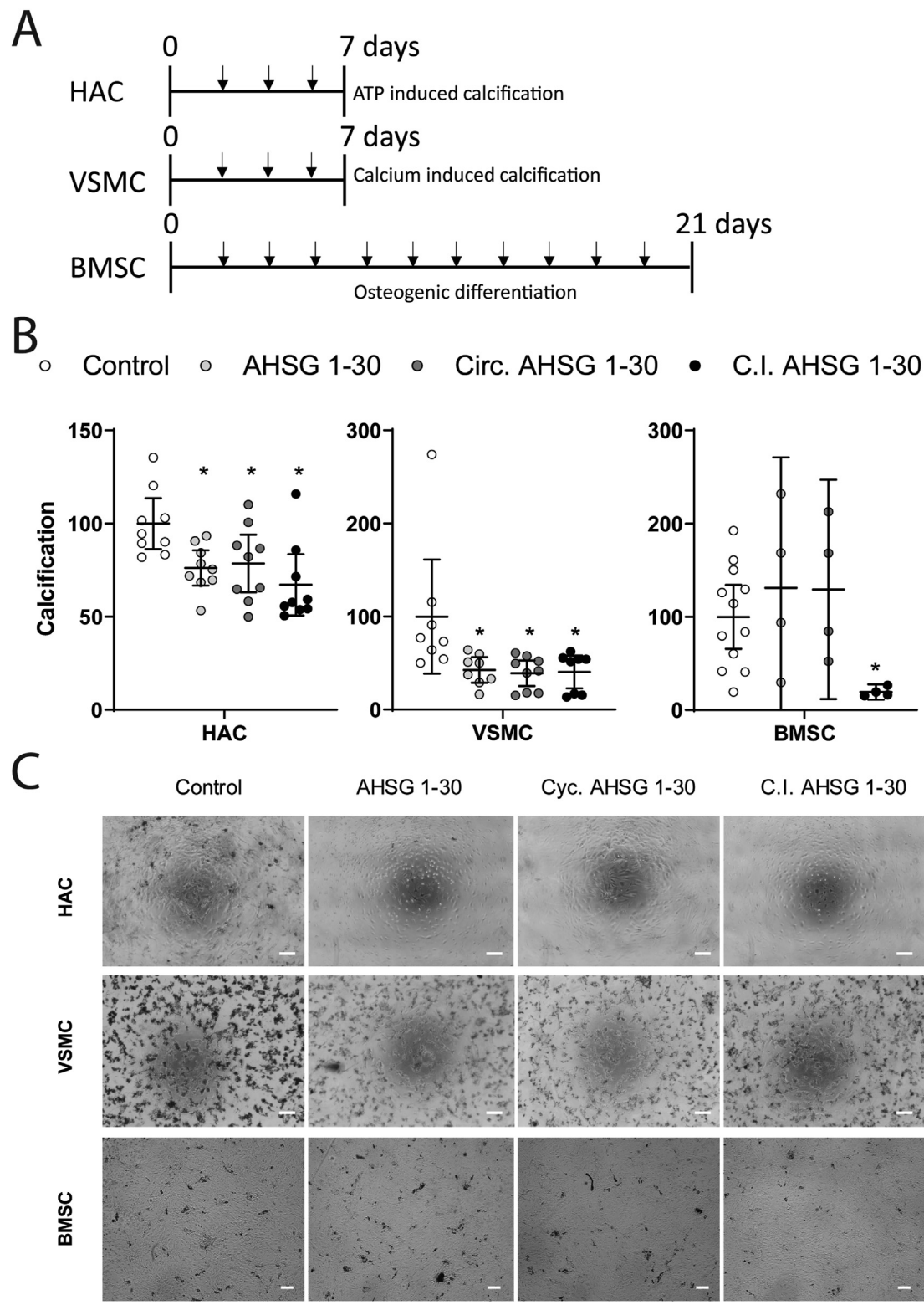


Fig. 5

observed inhibition plateau at these concentrations is reminiscent of the one observed in Tris/HCl at lower concentrations (Cf. Fig. 2).

Cyclic AHSG 1–30 peptide inhibits calcification in multiple cellular models

To test if the AHSG 1–30 peptide variants showed *in vivo* anti-calcification properties, we tested their effect in three different well-established calcification models [Fig. 5(A);^{42–44}]. We found 22–33% inhibition of calcification of HACs with the three peptide variants [Fig. 5(B); left panel]. In the VSMC calcification model, we found 58–61% inhibition of calcification with the peptides [Fig. 5(B); middle panel]. Finally, in the BMSC osteogenic differentiation model, only the C.I. peptide showed strong inhibition (81%) of calcification [Fig. 5(B); right panel]. Osteogenic differentiation of BMSC was confirmed with Alizarin Red staining and gene expression analysis (Supplemental Fig. 2). The peptide treatment effect was clearly visible as a reduction of black precipitates in phase-contrast images [Fig. 5(C)].

Cartilage degeneration reduced and mobility improved by C.I. AHSG 1–30 in rat osteoarthritis

Since BCP and CPPD crystals are detected in human end-stage osteoarthritis and injection of BCP crystals exacerbates OA in rodent models^{3,6,45–47}, we evaluated the effect of bi-weekly intra-articular (i.a.) injection of the C.I. AHSG 1–30 peptide in a rat osteoarthritis model³⁴. Histological assessment of the treated knee joints revealed a moderate but consistent decrease in fibrillation and cartilage lesion size in the treatment group [Fig. 6(A)]. Additional immunohistochemical staining revealed retention of Collagen type II in the medial tibial cartilage defect in the treatment group, when compared to the larger defect in controls where this was reduced. Alkaline phosphatase (ALP) positive chondrocytes were identified at the opposing femur cartilage in the deep zone. Collagen type I localized to bone tissue and was hardly detectable in articular cartilage. Few cell bodies stained positive for DIPEN, usually in close proximity to the site of damage or in the opposing femur in the deep cartilage zone, while larger positive areas appeared to be aspecific. There was no apparent difference between the groups for ALP, Collagen type I or DIPEN staining. Histopathological scoring at 28 days post OA induction revealed a 38% reduction in OA score between treatment and control groups [Fig. 6(B)]. Upon closer examination we found that the depth ratio in the most affected articular cartilage region was significantly reduced by the treatment compared to control [Fig. 6(C)]. A trend towards reduction with peptide treatment was identified for cartilage and severe to mild collagen degeneration in comparison to control. Concomitantly, there was a large improvement in gait score between treatment and control groups with 14/20 animals having a normal gait, while only 5/20 animals had a normal gait in the control group [Fig. 6(D)]. To test for potential systemic side effects of the treatment, we evaluated the concentration of 23 cytokines,

C-reactive protein (CRP), calcium, phosphate, ALP activity and total protein in rat sera obtained at 28 days post OA induction (Table II). Serum interferon γ (IFN γ) was significantly reduced by 9% in peptide treated animals [Fig. 6(D)]. A trend towards reduced RANTES (7%) and IL-5 (5%) levels was found as well. IFN γ was significantly correlated to OA histopathology score [Supplemental Fig. 4(B): $r = 0.45$; $N = 40$, P value = 0.0036].

Discussion

Previously, truncation mutants of the AHSG Cystatin 1 domain were generated by bacterial expression and purification^{16,17}. A minimum length of 40 AA (42–81 of Ahsg) could inhibit calcium phosphate precipitation *in vitro* by 50%¹⁷, while AA 1–51 and AA 42–70 of Ahsg did not show inhibitory potential¹⁶. Moreover, a synthesized 20 amino acid peptide spanning AA 62–81 was also not effective¹⁶. Therefore, the activity of our AHSG 1–30 peptide was unexpected. We speculate that improvements in peptide synthesis and purification methods have allowed us to investigate this in greater detail than previously possible. The amino acid sequence of the 1–30 peptide appears to be important for the inhibition of calcium phosphate precipitation. The first or last 4 AA of the peptide also appeared to be instrumental to achieve >60% precipitation inhibition (Supplementary Fig. 1). Cyclization improved the precipitation inhibition potency of the AHSG 1–30 peptide tremendously. We suspect that a more constrained peptide structure enhances the interaction of the Cyclic AHSG 1–30 peptide with either calcium ions, nucleation centers or primary CPP. We speculate that μ M inhibition depends partially on binding to calcium ions and that a distinct mechanism becomes dominant at lower concentrations. Based on protein measurements in the washed precipitates we concluded that this requires interaction of the peptide with the crystal. The similar amount of calcium and phosphate in precipitates derived from incubation with bFetuin or Cyclic AHSG 1–30 suggests a similar mode of action.

The linear, Cyclic, and C.I. variant of the AHSG 1–30 peptide were evaluated in three cellular models of calcification. Although we found that inhibition of calcification by the peptide is reduced in more complex solutions, the C.I. peptide convincingly reduced cellular calcification up to 3 weeks in BMSC osteogenesis. A previously identified 12 AA peptide, designed to bind hydroxyapatite (HA) to improve cell–HA interactions, was able to inhibit phosphate-induced MC3T3-E1 mineralization *in vitro*⁴⁸. This 12-mer HA-binding peptide had a 10-fold increased affinity for HA upon phosphorylation of its first three AA. It was found that net charge and phosphorylation were the most important for HA binding, while the actual sequence was also important for inhibition of mineralization. In an earlier paper on this 12 AA peptide, a concentration of 100 μ M showed 30% inhibition of mineralization and lower concentrations were unfortunately not reported⁴⁹. Notably, our AHSG 1–30 peptide variants were effective at much lower molar concentrations in both calcium-induced and phosphate-induced calcification models.

Inhibition of cellular calcification by variants of the AHSG 1–30 peptide. A) Experimental setup of three cellular calcification models. HACs were stimulated for 7 days with 1 mM ATP and with or without 20.7 μ M of the indicated peptides. VSMCs were stimulated for 7 days with 4.5 mM calcium ions in the presence or absence of 20.7 μ M of indicated peptides. BMSCs were differentiated for 21 days in differentiation medium containing BGP in the presence or absence of 2.1 μ M of indicated peptides. B) Quantification of total calcium deposition per well (Randox Calcium assay, normalized to total protein). BMSC; 1 donor with 4 biological replicates was used ($n = 12$ for Control). HACs and VSMCs; 3 donors with 3 biological replicates. Three samples were not detectable in VSMC calcification in three different treatment groups and are therefore not shown. For each donor the positive control was normalized to 100%. * = P value < 0.05 in a one-way ANOVA with Dunnett's post-test when compared to control. Mean \pm 95% confidence interval. C) Phase-contrast images were obtained at the final day of each experiment. Macroscopic calcifications can be seen as black dots⁶³. One representative image is shown per condition. Scale bars indicate 200 μ m.

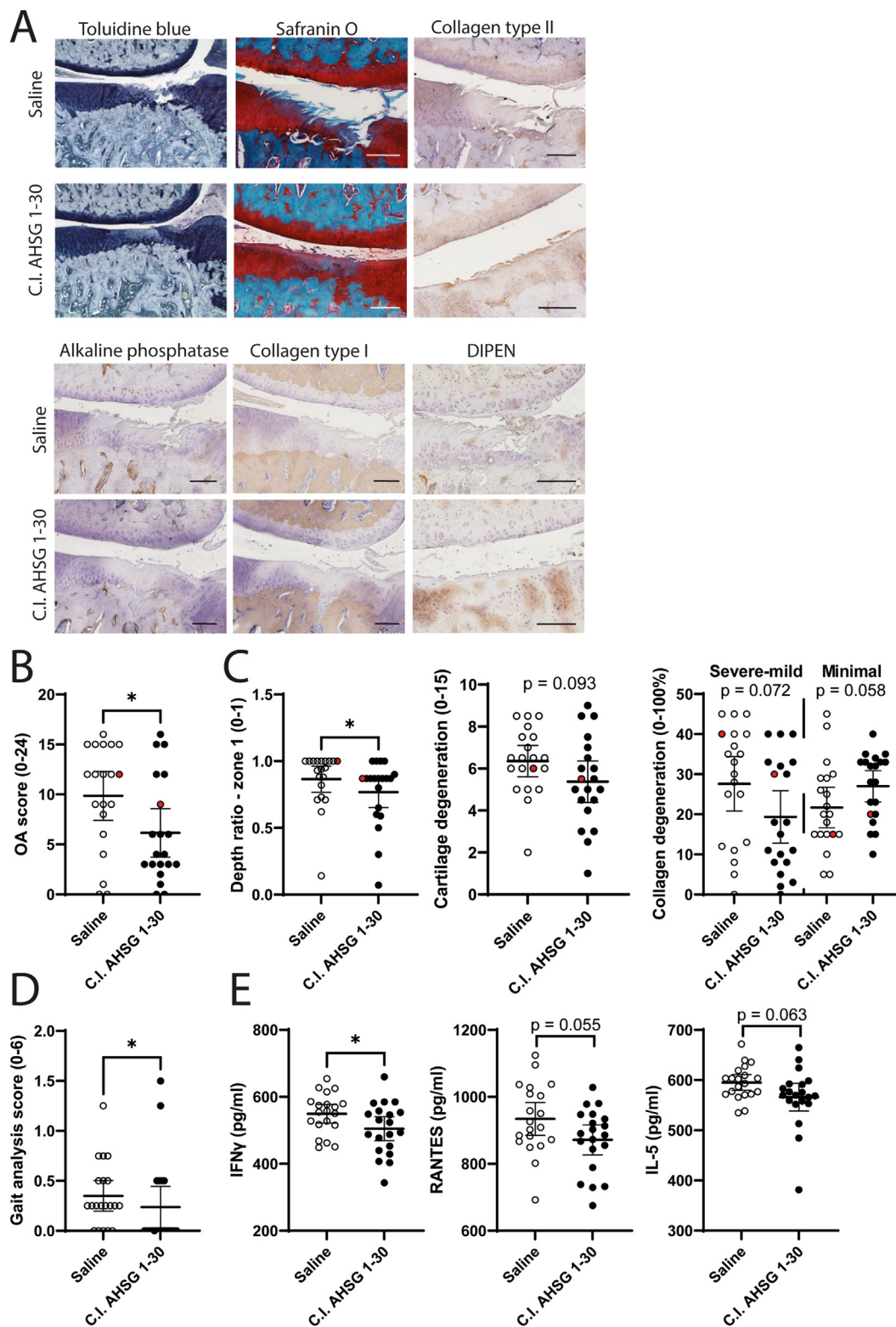


Fig. 6

Parameter (pg/ml USO)	Saline (Mean + 95% C.I.)	C.I. AHSG 1–30 (Mean + 95% C.I.)	P-value
IL1- α	220.3 (210.0–230.6)	211.6 (201.2–222.0)	0.224
IL1- β	819.9 (551.4–1088)	636.3 (498.7–773.9)	0.211
IL-2	1644 (1569–1719)	1584 (1491–1676)	0.293
IL-4	303.1 (289.4–316.7)	293.4 (279.5–307.3)	0.305
IL-5	595.2 (579.4–611)	566.1 (538.6–593.6)	0.063
IL-6	425.2 (380.8–469.5)	390.5 (338.4–442.6)	0.296
IL-7	661.2 (459.0–863.3)	535.0 (416.9–653.0)	0.266
IL-10	143.8 (136.3–151.3)	139.2 (132.0–146.5)	0.367
IL-12 (p70)	386.8 (367.4–406.3)	375.6 (347.8–403.4)	0.493
IL-13	190.6 (166.5–214.6)	195.1 (161.0–229.2)	0.820
IL-17A	60.2 (55.1–65.3)	57.0 (54.0–60.0)	0.269
IL-18	2577 (2242–2913)	3468 (2299–4636)	0.134
G-CSF	11.4 (9.4–13.5)	17.7 (3.6–31.8)	0.363
GM-CSF	592.5 (406.0–779.0)	460.5 (359.6–561.4)	0.200
GRO/KC	243.6 (200.8–286.3)	213.9 (189.3–238.6)	0.217
IFN- γ	549.4 (521.3–577.4)	504.6 (468.5–540.6)	0.047*
M-CSF	31.2 (27.5–34.9)	33.3 (29.6–37.0)	0.402
MIP-1 α	223.8 (131.6–316.0)	161.7 (123.1–200.3)	0.202
MIP-3 α	31.4 (26.8–36.0)	27.2 (24.8–29.6)	0.100
RANTES	934.2 (885.2–983.2)	871.6 (827.0–916.2)	0.055
TNF- α	932.6 (868.4–996.9)	917.7 (818.3–1017.0)	0.794
VEGF	164.5 (127.9–201.1)	142.3 (117.4–167.2)	0.301
MCP-1	2250 (1729–2770)	1850 (1599–2100)	0.156
CRP (μ g/ml)	1091.9 (1051–1133)	1122.1 (1113–1152)	0.221
Calcium (mM)	3.23 (3.14–3.31)	3.21 (3.17–3.28)	0.772
Phosphate (mM)	2.55 (2.32–2.66)	2.48 (2.25–2.53)	0.250
Protein (mg/ml)	54.88 (53.84–55.92)	54.84 (53.69–55.99)	0.958
ALP activity (μ mol/g/min)	0.326 (0.306–0.346)	0.341 (0.326–0.356)	0.221

Table II

Osteoarthritis and Cartilage

Serum measurements in the MCLT + MMT OA rat model at day 28

Macroscopic calcifications are always found in end-stage human osteoarthritis, and BCP crystals were shown to exacerbate OA in rodent model systems³. Calcium-containing crystals can induce synovial inflammation and chondrocyte apoptosis. It is currently not known what role microscopic calcifications, in the form of secondary CPPs, play in initiation or progression of OA. These microscopic calcifications are notoriously difficult to detect. Two correlations were recently found between lower limb arterial calcification or aortic valve calcification and OA^{50,51}. This links a systemic susceptibility to calcification to OA. In our Lewis rat OA model, we focused on standard outcome parameters to assess the effect of intra-articular peptide administration³⁴. However, a study limitation is that calcification has not been confirmed in this particular model in this rat strain. In Sprague–Dawley rats large

macroscopic calcifications occur in articular cartilage at 9–12 months of age and this may affect friction, wear, and lubrication of the knee joint⁵². Our developed peptide might be tested in such an ageing model for calcification or in a more acute loading induced mouse model for joint calcification⁵³. In addition, it would be desirable to assess the effect of continuous administration of our developed D-amino acid peptide on healthy cartilage over a longer time course to evaluate biosafety. We found a significant reduction on osteoarthritis score and improvement on gait score that reflects animal mobility and pain-related behavior⁵⁴. Intra-peritoneal injections with phosphocitrate in guinea pigs was shown to reduce cartilage damage induced by a partial meniscectomy⁵⁵. Injection of sodium thiosulphate in mice was shown to reduce OA cartilage score⁵⁶. However, sodium thiosulphate was reported to induce

Intra-articular injection of C.I. AHSG 1–30 ameliorates osteoarthritis score and animal mobility in a rat osteoarthritis model. An *in vivo* MCLT + MMT osteoarthritis model with 20 rats per group was performed. Bi-weekly intra-articular injections of 50 μ l peptide with a concentration of 20 μ M or 50 μ l saline were performed. Gait was analyzed at day 20 and animals were sacrificed at day 28, followed by histological analysis. Peptide treatment did not affect total body weight [Supplemental Fig. 4(A)]. A) Representative toluidine blue, Safranin O, Collagen type II, Collagen type I, ALP and neopeptide DIPEN IHC stainings for each group. B) Osteoarthritis score. Each dot represents one animal, red dots correspond to the animals shown in A. Mean \pm 95% confidence interval ($n = 20$). * = P value < 0.05 in a Mann–Whitney U test. C) Medial tibia zone 1 depth ratio, cartilage degeneration score (total of zone 1–3) and collagen degeneration severe-mild and minimal are presented in separate graphs. Red dots correspond to the animals shown in A. Mean \pm 95% confidence interval ($n = 20$). * = P value < 0.05 in a Mann–Whitney U test. D) Gait analyses score. Mean \pm 95% confidence interval ($n = 20$). * = P value < 0.05 in a Mann–Whitney U test. E) IFN γ , RANTES and IL-5 serum levels as determined by Luminex assay. Mean \pm SEM ($n = 20$). * = P value < 0.05 (Student t -test). Additional serum measurements can be found in Table II. Body weight and the IFN γ correlation plot with OA score can be found in Supplemental Fig. 4.

undesirable acidosis-induced bone resorption in rats⁵⁷. We found a significant reduction in serum IFN γ levels following peptide treatment and a correlation with OA histopathology. IFN γ was increased in synovial fluid 2 years post anterior cruciate ligament injury⁵⁸ and also in synovial fluid immediately after i.a. proximal knee fracture⁵⁹. Interestingly, patient reported acute knee pain was significantly correlated to IFN γ in knee lavages ($r = 0.6$, $N = 70$, P value < 0.05)⁶⁰. In sera from early OA patients compared to advanced OA, IL-5 was significantly higher and IFN γ showed a similar trend⁶¹. We did not observe systemic alterations of other cytokines or chemical parameters.

The C.I. AHS 1–30 peptide is the first i.a. injection therapy that was designed to ameliorate pathological calcification and for which we observed a reduced experimental OA histopathology. In humans, histological cartilage degeneration (OARSI score) was shown to correlate with calcification of the knee⁶². Therefore, positive effects on histological parameters combined with the improvement in gait can be seen as promising for this type of intervention. Future studies should focus on calcification models, such as the murine knee joint compression model⁵³, or vascular calcification and kidney failure models to assess the benefit of the C.I. AHS 1–30 peptide across calcification disorders.

Ethics statement

This study complies with the Declaration of Helsinki. Surgical waste material of total knee replacement surgery of end-stage osteoarthritis patients was obtained after informed consent (METC 2017-0183). Bone marrow aspirates from the iliac crest of young individuals (METC 08-4-056) was used for BMSC isolation. Human aortic samples were obtained as surgical waste material from patients undergoing open aortic surgery in accordance with the Dutch Code for Proper Secondary Use of Human Tissue (<http://www.fmwv.nl>). The animal study design and animal usage was approved by BBP's Institutional Animal Care and Use Committee (IACUC) for compliance with regulations prior to study initiation (IACUC Protocol No. BBP-008). Animal husbandry, weighing, randomization, dose preparation and dosing, behavioral testing, blood collection, and necropsies were performed by BBP personnel who were trained in the proper procedures and approved by BBP's IACUC. An attending veterinarian was on site or on call during the live phase of the study. Animal care including room, cage, and equipment sanitation conformed to the guidelines cited in the Guide for the Care and Use of Laboratory Animals (Guide, 2011).

Author contributions

Conceptualization: GA, MC, LS, TW. Methodology: GA, JS, RS, GW, KW, MC, LP. Investigation: GA, JS, RS, GW, KW, MC, LP. Visualization: GA, JS, RS, GW. Funding acquisition: MC, TW, LR. Project administration: GA, JS, RS, GW. Supervision: LS, LR, TW. Writing - original draft: GA, JS, RS, GW. Writing - review & editing: GA, JS, RS, GW, MC, LS, LR, TW.

Conflict of interest

GA, LS, LR and TW are inventors on a patent application regarding the here described work (AOMB 80484EP). MC and TW are inventors on patents WO2017178251 and WO2017178253 (owned by Chondropeptix). LR and TW are shareholders in Chondropeptix and are CDO and CSO of Chondropeptix, respectively. LS is stockholders in Coagulation Profile.

Role of the funding source

This work was financially supported by a grant from Stichting de Weijerhorst (project: Bewegen zonder Pijn) and a grant from the Dutch Arthritis Association (LLP14). The work of Dr. Schurgers was

supported by the Norwegian Research Council 241584 and by the European Union's Horizon 2020 research and innovation programmes under the Marie Skłodowska-Curie grant agreement No 722609, 764474, and 813409.

Acknowledgments

We would to thank Hans Duimel from the microscopy CORE lab at Maastricht University for assistance with SEM imaging, Dr Marije Koenders from the dept. of Experimental Rheumatology at the Radboudumc Nijmegen for assistance with the Luminex assay.

Supplementary data

Supplementary data to this article can be found online at <https://doi.org/10.1016/j.joca.2022.11.007>.

References

- Jaminon A, Reesink K, Kroon A, Schurgers L. The role of vascular smooth muscle cells in arterial remodeling: focus on calcification-related processes. *Int J Mol Sci* 2019;20(22):5694, <https://doi.org/10.3390/ijms20225694>.
- Mulay SR, Anders H-J. Crystal nephropathies: mechanisms of crystal-induced kidney injury. *Nat Rev Nephrol* 2017;13(4):226–40, <https://doi.org/10.1038/nrneph.2017.10>.
- McCarthy GM, Dunne A. Calcium crystal deposition diseases — beyond gout. *Nat Rev Rheumatol* 2018;14(10):592–602, <https://doi.org/10.1038/s41584-018-0078-5>.
- Mortensen JD, Baggenstoss AH. Nephrocalcinosis: a review. *Am J Clin Pathol* 1954;24(1):45–63, <https://doi.org/10.1093/ajcp/24.1.45>.
- McCarty D. Crystals, joints, and consternation. *Ann Rheum Dis* 1983;42(3):243–53, <https://doi.org/10.1136/ard.42.3.243>.
- Conway R, McCarthy GM. Calcium-containing crystals and osteoarthritis: an unhealthy alliance. *Curr Rheumatol Rep* 2018;20(3):13, <https://doi.org/10.1007/s11926-018-0721-9>.
- Molloy ES, McCarthy GM. How crystals damage tissue. *Curr Rheumatol Rep* 2004;6(3):228–34, <https://doi.org/10.1007/s11926-004-0073-5>.
- Ea HK, Chobaz V, Nguyen C, Nasi S, van Lent P, Daudon M, et al. Pathogenic role of basic calcium phosphate crystals in destructive arthropathies. *PLoS One* 2013;8(2), e57352, <https://doi.org/10.1371/journal.pone.0057352> [published Online First: 2013/03/08].
- Meyer F, Dittmann A, Kornak U, Herbster M, Pap T, Lohmann CH, et al. Chondrocytes from osteoarthritic and chondrocalcinosis cartilage represent different phenotypes. *Front Cell Dev Biol* 2021;9, 622287, <https://doi.org/10.3389/fcell.2021.622287> [published Online First: 2021/05/14].
- Jafri L, Khan AH, Azeem S. Ionized calcium measurement in serum and plasma by ion selective electrodes: comparison of measured and calculated parameters. *Indian J Clin Biochem* 2014;29(3):327–32, <https://doi.org/10.1007/s12291-013-0360-x> [published Online First: 2013/07/25].
- Stock M, Schett G. Vitamin K-dependent proteins in skeletal development and disease. *Int J Mol Sci* 2021;22(17), <https://doi.org/10.3390/ijms22179328> [published Online First: 2021/09/11].
- Häusler M, Schäfer C, Osterwinter C, Jähnen-Dechent W. The physiologic development of fetuin-A serum concentrations in children. *Pediatr Res* 2009;66(6):660–4, <https://doi.org/10.1203/DR.0b013e3181bc3f60>.
- Brylka L, Jähnen-Dechent W. The role of fetuin-A in physiological and pathological mineralization. *Calcif Tissue Int*

- 2013;93(4):355–64, <https://doi.org/10.1007/s00223-012-9690-6>.
14. Schafer C, Heiss A, Schwarz A, Westenfeld R, Ketteler M, Floege J, et al. The serum protein alpha 2-Heremans-Schmid glycoprotein/fetuin-A is a systemically acting inhibitor of ectopic calcification. *J Clin Invest* 2003;112(3):357–66, <https://doi.org/10.1172/JCI17202>.
15. Pedersen KO. Fetuin, a new globulin isolated from serum. *Nature* 1944;154(3914):575, <https://doi.org/10.1038/154575a0>.
16. Schinke T, Amendt C, Trindl A, Pöschke O, Müller-Esterl W, Jahnhen-Dechent W. The serum protein α 2-HS glycoprotein/fetuin inhibits apatite formation in vitro and in mineralizing calvaria cells: a possible role in mineralization and calcium homeostasis. *J Biol Chem* 1996;271(34):20789–96, <https://doi.org/10.1074/jbc.271.34.20789>.
17. Heiss A, DuChesne A, Denecke B, Grötzinger J, Yamamoto K, Renné T, et al. Structural basis of calcification inhibition by α 2-HS glycoprotein/fetuin-A: formation of colloidal calciprotein particles. *J Biol Chem* 2003;278(15):13333–41, <https://doi.org/10.1074/jbc.M210868200>.
18. Zeper LW, de Baaij JHF. Magnesium and calciprotein particles in vascular calcification: the good cop and the bad cop. *Curr Opin Nephrol Hypertens* 2019;28(4):368–74, <https://doi.org/10.1097/mnh.0000000000000509>.
19. Köppert S, Büscher A, Babler A, Ghallab A, Buhl EM, Latz E, et al. Cellular clearance and biological activity of calciprotein particles depend on their maturation state and crystallinity. *Front Immunol* 2018;9:1991, <https://doi.org/10.3389/fimmu.2018.01991> [published Online First: 2018/09/21].
20. Dervisoglu E, Kir HM, Kalender B, Caglayan C, Eraldemir C. Serum fetuin-A concentrations are inversely related to cytokine concentrations in patients with chronic renal failure. *Cytokine* 2008;44(3):323–7, <https://doi.org/10.1016/j.cyto.2008.08.014>.
21. Zhou Z, Ji Y, Ju H, Chen H, Sun M. Circulating fetuin-A and risk of all-cause mortality in patients with chronic kidney disease: a systematic review and meta-analysis. *Front Physiol* 2019;10:966, <https://doi.org/10.3389/fphys.2019.00966> [published Online First: 2019/08/17].
22. Laugsand LE, Ix JH, Bartz TM, Djousse L, Kizer JR, Tracy RP, et al. Fetuin-A and risk of coronary heart disease: a Mendelian randomization analysis and a pooled analysis of AHSG genetic variants in 7 prospective studies. *Atherosclerosis* 2015;243(1):44–52, <https://doi.org/10.1016/j.atherosclerosis.2015.08.031> [published Online First: 2015/09/08].
23. Cahalane RM, Barrett HE, Ross AM, Mulvihill JJE, Purtill H, Selvarajah L, et al. On the association between circulating biomarkers and atherosclerotic calcification in a cohort of arterial disease participants. *Nutr Metab Cardiovasc Dis* 2021;31(5):1533–41, <https://doi.org/10.1016/j.numecd.2021.02.005> [published Online First: 2021/04/04].
24. Timur UT, Jahr H, Anderson J, Green DC, Emans PJ, Smagul A, et al. Identification of tissue-dependent proteins in knee OA synovial fluid. *Osteoarthritis Cartilage* 2021;29(1):124–33, <https://doi.org/10.1016/j.joca.2020.09.005> [published Online First: 2020/11/10].
25. Favero M, Belluzzi E, Frallonardo P, Peruzzo L, Tauro L, Oliviero F, et al. Synovial fluid fetuin-A levels in patients affected by osteoarthritis with or without evidence of calcium crystals. *Rheumatology* 2019;58(4):729–30, <https://doi.org/10.1093/rheumatology/key435>.
26. Walters ME, Esfandi R, Tsopmo A. Potential of food hydrolyzed proteins and peptides to chelate iron or calcium and enhance their absorption. *Foods* 2018;7(10):172, <https://doi.org/10.3390/foods7100172>.
27. Huang S-L, Zhao L-N, Cai X, Wang S-Y, Huang Y-F, Hong J, et al. Purification and characterisation of a glutamic acid-containing peptide with calcium-binding capacity from whey protein hydrolysate. *J Dairy Res* 2015;82(1):29–35, <https://doi.org/10.1017/S0022029914000715> [published Online First: 2015/01/16].
28. Wang L, Ding Y, Zhang X, Li Y, Wang R, Luo X, et al. Isolation of a novel calcium-binding peptide from wheat germ protein hydrolysates and the prediction for its mechanism of combination. *Food Chem* 2018;239:416–26, <https://doi.org/10.1016/j.foodchem.2017.06.090>.
29. Hou T, Wang C, Ma Z, Shi W, Weiwei L, He H. Desalted duck egg white peptides: promotion of calcium uptake and structure characterization. *J Agric Food Chem* 2015;63(37):8170–6, <https://doi.org/10.1021/acs.jafc.5b03097>.
30. Cai X, Lin J, Wang S. Novel peptide with specific calcium-binding capacity from Schizochytrium sp. protein hydrolysates and calcium bioavailability in Caco-2 cells. *Mar Drugs* 2016;15(1):3, <https://doi.org/10.3390/md15010003>.
31. Cai MMX, Smith ER, Holt SG. The role of fetuin-A in mineral trafficking and deposition. *Bonekey Rep* 2015;4:672, <https://doi.org/10.1038/bonekey.2015.39>.
32. Neradova A, Wasilewski G, Prisco S, Leenders P, Caron M, Welting T, et al. Combining phosphate binder therapy with vitamin K2 inhibits vascular calcification in an experimental animal model of kidney failure. *Nephrol Dial Transplant* 2022;37(4):652–62, <https://doi.org/10.1093/ndt/gfab314> [published Online First: 2021/11/01].
33. Peffers MJ, Chabronova A, Balaskas P, Fang Y, Dyer P, Cremers A, et al. SnoRNA signatures in cartilage ageing and osteoarthritis. *Sci Rep* 2020;10(1), 10641, <https://doi.org/10.1038/s41598-020-67446-z> [published Online First: 2020/07/02].
34. Janusz MJ, Bendele AM, Brown KK, Taiwo YO, Hsieh L, Heitmeyer SA. Induction of osteoarthritis in the rat by surgical tear of the meniscus: inhibition of joint damage by a matrix metalloproteinase inhibitor. *Osteoarthritis Cartilage* 2002;10(10):785–91, <https://doi.org/10.1053/joca.2002.0823> [published Online First: 2002/10/03].
35. Caron MMJ, Ripmeester EGJ, van den Akker G, Wijnands N, Steijns J, Surtel DAM, et al. Discovery of bone morphogenetic protein 7-derived peptide sequences that attenuate the human osteoarthritic chondrocyte phenotype. *Mol Ther Methods Clin Dev* 2021;21:247–61, <https://doi.org/10.1016/j.omtm.2021.03.009> [published Online First: 2021/04/15].
36. Kumar A, Bendele AM, Blanks RC, Bodick N. Sustained efficacy of a single intra-articular dose of FX006 in a rat model of repeated localized knee arthritis. *Osteoarthritis Cartilage* 2015;23(1):151–60, <https://doi.org/10.1016/j.joca.2014.09.019> [published Online First: 2014/10/01].
37. Pritzker KPH, Gay S, Jimenez SA, Ostergaard K, Pelletier JP, Revell PA, et al. Osteoarthritis cartilage histopathology: grading and staging. *Osteoarthritis Cartilage* 2006;14(1):13–29, <https://doi.org/10.1016/j.joca.2005.07.014>.
38. Gerwin N, Bendele AM, Glasson S, Carlson CS. The OARSI histopathology initiative - recommendations for histological assessments of osteoarthritis in the rat. *Osteoarthritis Cartilage* 2010;18(Suppl 3):S24–34, <https://doi.org/10.1016/j.joca.2010.05.030> [published Online First: 2010/10/01].
39. Steinbusch MMF, Caron MMJ, Surtel DAM, van den Akker GGH, van Dijk PJ, Friedrich F, et al. The antiviral protein viperin regulates chondrogenic differentiation via CXCL10 protein secretion. *J Biol Chem* 2019;294(13):5121–36, <https://doi.org/10.1074/jbc.RA119.007356> [published Online First: 2019/02/06].
40. Koehnke J, Naismith J, van der Donk W. *Cyclic Peptides: From Bioorganic Synthesis to Applications*. Royal Society of Chemistry; 2017.

41. Ng S, Guo J, Ma J, Loo SC. Synthesis of high surface area meso-structured calcium phosphate particles. *Acta Biomater* 2010;6(9):3772–81, <https://doi.org/10.1016/j.actbio.2010.03.017> [published Online First: 2010/03/18].
42. Kapustin AN, Chatrou MLL, Drozdov I, Zheng Y, Davidson SM, Soong D, et al. Vascular smooth muscle cell calcification is mediated by regulated exosome secretion. *Circ Res* 2015;116(8):1312–23, <https://doi.org/10.1161/CIRCRESAHA.116.305012>.
43. Jubeck B, Muth E, Gohr CM, Rosenthal AK. Type II collagen levels correlate with mineralization by articular cartilage vesicles. *Arthritis Rheum* 2009;60(9):2741–6, <https://doi.org/10.1002/art.24773>.
44. Maniopoulos C, Sodek J, Melcher AH. Bone formation in vitro by stromal cells obtained from bone marrow of young adult rats. *Cell Tissue Res* 1988;254(2):317–30, <https://doi.org/10.1007/BF00225804>.
45. Ea H-K, Nguyen C, Bazin D, Bianchi A, Guicheux J, Reboul P, et al. Articular cartilage calcification in osteoarthritis: insights into crystal-induced stress. *Arthritis Rheum* 2011;63(1):10–8, <https://doi.org/10.1002/art.27761>.
46. Mitsuyama H, Healey RM, Terkeltaub RA, Coutts RD, Amiel D. Calcification of human articular knee cartilage is primarily an effect of aging rather than osteoarthritis. *Osteoarthritis Cartilage* 2007;15(5):559–65, <https://doi.org/10.1016/j.joca.2006.10.017> [published Online First: 2007/02/06].
47. Pauli C, Grogan SP, Patil S, Otsuki S, Hasegawa A, Koziol J, et al. Macroscopic and histopathologic analysis of human knee menisci in aging and osteoarthritis. *Osteoarthritis Cartilage* 2011;19(9):1132–41, <https://doi.org/10.1016/j.joca.2011.05.008> [published Online First: 2011/06/21].
48. Ramaswamy J, Nam HK, Ramaraju H, Hatch NE, Kohn DH. Inhibition of osteoblast mineralization by phosphorylated phage-derived apatite-specific peptide. *Biomaterials* 2015;73:120–30, <https://doi.org/10.1016/j.biomaterials.2015.09.021> [published Online First: 2015/09/15].
49. Addison WN, Miller SJ, Ramaswamy J, Mansouri A, Kohn DH, McKee MD. Phosphorylation-dependent mineral-type specificity for apatite-binding peptide sequences. *Biomaterials* 2010;31(36):9422–30, <https://doi.org/10.1016/j.biomaterials.2010.08.064> [published Online First: 2010/10/12].
50. Karaali E, Çiloğlu O, Yücel C, Ekiz T. The relationship between primary knee osteoarthritis and aortic stiffness, distensibility, and valve calcifications: a case-control study. *J Clin Rheumatol* 2022;28(1):e9–e12, <https://doi.org/10.1097/rhu.0000000000001568> [published Online First: 2020/09/15].
51. Yoshida S, Nishitani K, Yamamoto Y, Ito H, Saito M, Morita Y, et al. Association between quantitative lower limb arterial calcification and bilateral severe knee osteoarthritis. *Mod Rheumatol* 2021;31(5):1059–65, <https://doi.org/10.1080/14397595.2020.1868120> [published Online First: 2021/01/08].
52. Roemhildt ML, Beynon BD, Gardner-Morse M. Mineralization of articular cartilage in the Sprague-Dawley rat: characterization and mechanical analysis. *Osteoarthritis Cartilage* 2012;20(7):796–800, <https://doi.org/10.1016/j.joca.2012.04.011> [published Online First: 2012/04/26].
53. Rai MF, Duan X, Quirk JD, Holguin N, Schmidt EJ, Chinzei N, et al. Post-traumatic osteoarthritis in mice following mechanical injury to the synovial joint. *Sci Rep* 2017;7: 45223, <https://doi.org/10.1038/srep45223> [published Online First: 2017/03/28].
54. Lakes EH, Allen KD. Gait analysis methods for rodent models of arthritic disorders: reviews and recommendations. *Osteoarthritis Cartilage* 2016;24(11):1837–49, <https://doi.org/10.1016/j.joca.2016.03.008> [published Online First: 2016/03/17].
55. Sun Y, Haines N, Roberts A, Ruffolo M, Mauerhan DR, Mihalko KL, et al. Disease-modifying effects of phosphocitrate and phosphocitrate- β -ethyl ester on partial meniscectomy-induced osteoarthritis. *BMC Musculoskelet Disord* 2015;16:270, <https://doi.org/10.1186/s12891-015-0724-x> [published Online First: 2015/10/02].
56. Nasi S, Ea H-K, Lioté F, So A, Busso N. Sodium thiosulfate prevents chondrocyte mineralization and reduces the severity of murine osteoarthritis. *PLoS One* 2016;11(7), e0158196, <https://doi.org/10.1371/journal.pone.0158196>.
57. Kenny J, Ostuni M, Musso CG. Is sodium thiosulfate an effective treatment for recurrent calcium nephrolithiasis? Pro and con arguments. *Int Urol Nephrol* 2018;50(10):1921–2, <https://doi.org/10.1007/s11255-018-1910-1>.
58. Roemer FW, Englund M, Turkiewicz A, Struglics A, Guermazi A, Lohmander LS, et al. Molecular and structural biomarkers of inflammation at two years after acute anterior cruciate ligament injury do not predict structural knee osteoarthritis at five years. *Arthritis Rheumatol* 2019;71(2):238–43, <https://doi.org/10.1002/art.40687>.
59. Holt I, Cooper RG, Denton J, Meager A, Hopkins SJ. Cytokine inter-relationships and their association with disease activity in arthritis. *Br J Rheumatol* 1992;31(11):725–33, <https://doi.org/10.1093/rheumatology/31.11.725> [published Online First: 1992/11/01].
60. Cuellar JM, Scuderi GJ, Cuellar VG, Golish SR, Yeomans DC. Diagnostic utility of cytokine biomarkers in the evaluation of acute knee pain. *JBJS* 2009;91(10).
61. Barker T, Rogers VE, Henriksen VT, Aguirre D, Trawick RH, Rasmussen GL, et al. Serum cytokines are increased and circulating micronutrients are not altered in subjects with early compared to advanced knee osteoarthritis. *Cytokine* 2014;68(2):133–6, <https://doi.org/10.1016/j.cyto.2014.04.004>.
62. Hubert J, Beil FT, Rolvien T, Butscheidt S, Hischke S, Püschel K, et al. Cartilage calcification is associated with histological degeneration of the knee joint: a highly prevalent, age-independent systemic process. *Osteoarthritis Cartilage* 2020;28(10):1351–61, <https://doi.org/10.1016/j.joca.2020.04.020> [published Online First: 2020/07/20].
63. Jaminon AMG, Akbulut AC, Rapp N, Kramann R, Biessen EAL, Temmerman L, et al. Development of the BioHybrid assay: combining primary human vascular smooth muscle cells and blood to measure vascular calcification propensity. *Cells* 2021;10(8), <https://doi.org/10.3390/cells10082097> [published Online First: 2021/08/28].